Optimal Survey Design Using Focused Resistivity Arrays

Elena Cherkaeva and Alan C. Tripp

Abstract— **The first problem which needs to be solved when planning any geoelectrical survey is a choice of a particular electrode configuration that can give the maximal response from a target inhomogeneity. We formulate a problem of maximizing the response as an optimization problem for an applied current intensity distribution on the surface. The solution of this problem is the optimal intensity distribution of the current, which maximizes the response from the inclusion. This problem is solved numerically with Singular Value Decomposition of an impedance matrix. The optimal current array is modeled as a current of varying optimal intensity injected at different electrodes. The problem does not need any information about the inclusion but its measured impedance matrix. Thus an optimal current array can be designed for every particular resistivity distribution. The optimal current patterns are found for a number of models of a conductive inclusion, and responses due to the optimal current are compared with responses due to conventional arrays. This method can be applied to any background and inclusion resistivity distribution.**

I. Introduction

THE direct current geoelectric prospecting technique has been used extensively in economic and scientific geological investigations. In any particular use, it is important to utilize all the power of the technique which it can provide. One way of doing this in borehole electrical logging is to use current focusing tools such as the Schlumberger "guarded electrode," focusing system of coils in induction logging [1], the Laterolog [2], and the Microlaterolog [3], [4]. These tools and more recent tools such as discussed by [5] and [6] have been developed for a particular purpose to wit they force the current into the formation perpendicular to the wall of the hole by maintaining equipotential distribution on the surface of a borehole. The same idea of maintaining constant potential values at different electrodes is used in [7] for synthetically focused resistivity measurements.

The choice of a particular array of transmitter and receiver electrodes to use in other geophysical and geotechnical applications have depended on model specific numerical experimental design in which the responses of various trial arrays were compared [8]. This technique is able to distinguish an optimal array for a given model among various trial arrays but is not capable of determining whether a better array exists.

Manuscript received September 22, 1994; revised February 14, 1995. This work was supported by DOE/OBES under Grant DE-FG03-93ER14313.

The authors are with the Department of Geology and Geophysics, University of Utah, Salt Lake City, UT 84112 USA.

Publisher Item Identifier S 0196-2892(96)01011-X.

This "trial and error" technique for comparing the efficacy of various electrode arrays is adequate for many applications, particularly if the geological setting of the target is very inhomogeneous or if logistical considerations require a very simple array. In these cases, finding an optimal array is either impossible due to lack of geological information or is irrelevant due to the practical problems in conducting the survey. However, we anticipate an increasing number of geological applications in which 1) the geological background may be fairly well characterized or in which measurements are differential in time and 2) the need for enhanced detecting or resolving capability will compensate for increased logistical difficulties. Such possible applications include monitoring water leakage at dam sites, monitoring contaminant plume migration, detecting buried "garbage" in a homogeneous fill material, or well-logging.

Given these possible applications, we have begun to examine the possibility of theoretically determining electrode arrays which are optimal for model detection or resolution given *a priori* information concerning the geological setting of the survey. A foundation for our work comes from work done in biomedical imaging and electrical tomography [9]–[12]. The mathematical background for our discussion is developed in [13] where this technique is applied to the problem of resolution and determining the reliability of a solution of an inverse problem for noisy measurements. In this paper, we adapt and extend the previous theoretical works to a geological setting. We present numerical experiments and show how injection current patterns which are optimal in detecting perturbations from an *a priori* model can be determined.

We use a system of pole-pole electrodes as a basis for construction of the optimal array. A similar technique can be exploited for utilizing other electrode arrays. The problem of maximizing the response from a target inhomogeneity is formulated as an optimization problem for an applied current intensity distribution on the surface. This problem is solved numerically with Singular Value Decomposition of an impedance matrix. The optimal current array is modeled as a set of currents of different intensity injected at different electrodes. The best current patterns are found for a number of models of a conductive inclusion, and responses due to the optimal current are compared with responses due to conventional arrays. This method can be applied to any background and inclusion resistivity distribution.

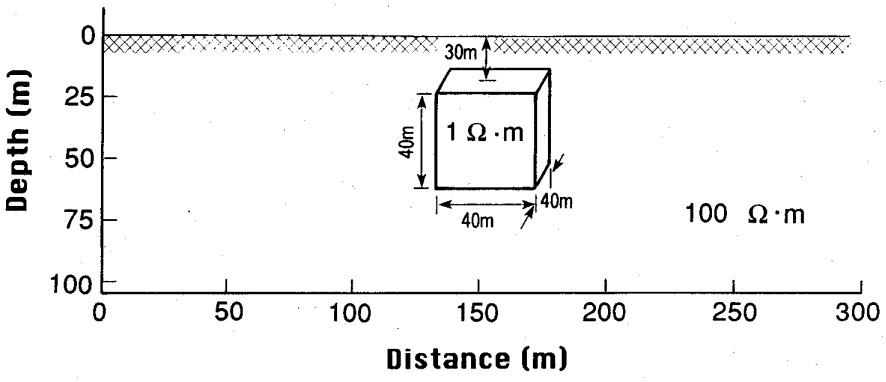

Fig. 1. Model A.

II. Mathematical Formulation of the Problem

A. Continuous Current Distributions

We introduce here the mathematical description of the problem. We consider the case of direct current injection. Let a domain $\mathcal{D}$ be a region of the Earth, on the surface $\partial\mathcal{D}$ of which is applied a current f.

The potentials and currents for the host medium γ and the perturbed medium $\gamma+\sigma$ satisfy the conductivity equations

$$\nabla\cdot(\gamma+\sigma)\nabla w=0 \text{ in } \mathcal{D},\quad (\gamma+\sigma)\frac{\partial w}{\partial n}=f \text{ on } \partial\mathcal{D} \quad (1)$$

and

$$\nabla\cdot\gamma\nabla u=0 \text{ in } \mathcal{D},\quad \gamma\frac{\partial u}{\partial n}=f \text{ on } \partial\mathcal{D}. \quad (2)$$

The potential values w and u are measured on the earth's surface and they are dependent on an array of injected currents f.

We consider the norm of the difference between response voltages w and u on the surface for the applied current f to be a measure of information content $\mathcal{I}$ of the specific data set, associated with the current f [11]:

$$\mathcal{I}^2=\|w-u\|^2_{L_2(\partial\mathcal{D})}=\int_{\partial\mathcal{D}}(w-u)^2. \quad (3)$$

The best current distribution on the surface is one that maximizes the response from the inclusion, i.e. maximizes the value $\mathcal{I}$,

$$M_1=\max_f \mathcal{I}(f)=\max_{f:\|f\|=1}\|w-u\|_{L_2(\partial\mathcal{D})}. \quad (4)$$

Likewise, the second best current distribution gives a value M_2, which is less than M_1 but is greater than all other values of $\mathcal{I}$. Continuing this process leads to a hierarchy of injection currents.

Equation (4) is an eigenvalue problem which has been considered in connection with the problem of distinguishability in a number of papers [9], [11], [12].

The currents are of unit norm because we wish to find the geometry of the optimal injection currents. Since the voltages scale with the current, larger voltage anomalies can always be found by uniformly increasing the magnitude of the injection currents.

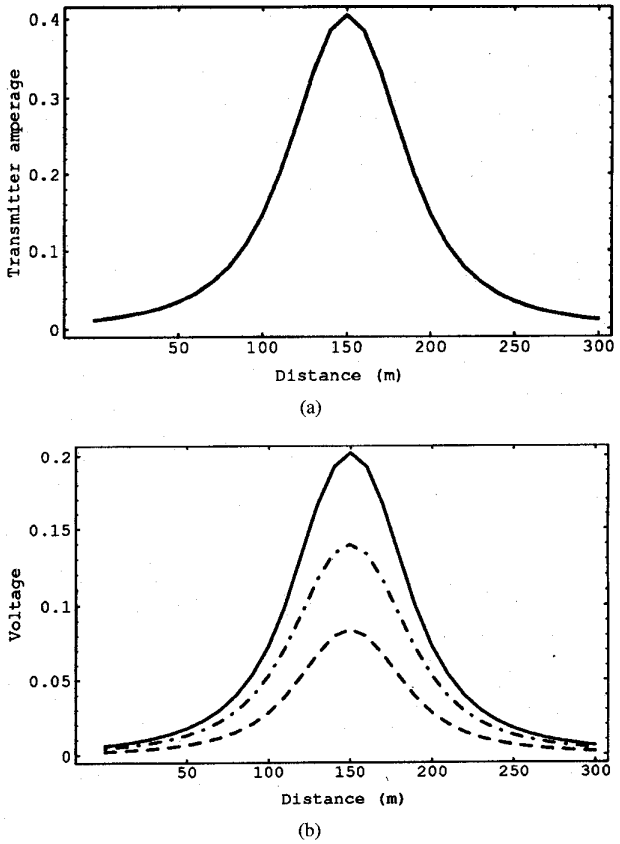

Fig. 2. Model A. A plot of the optimal transmitter (a) current intensity and (b) secondary responses for three different transmitter current patterns: 1) response of the optimal current (solid line); 2) response of the current of equal intensity at all electrodes (dot-dashed line); and 3) response of the unit current at the central electrode (dashed line).

Although statistical noise will influence array design for practical applications, we will not consider it here.

B. Construction of the Optimal Current Electrode Array

In actual field applications of the geoelectric technique, the transmitter and receiver electrodes are confined to a finite number of discrete points. Thus the theory for array optimization requires a matrix context.

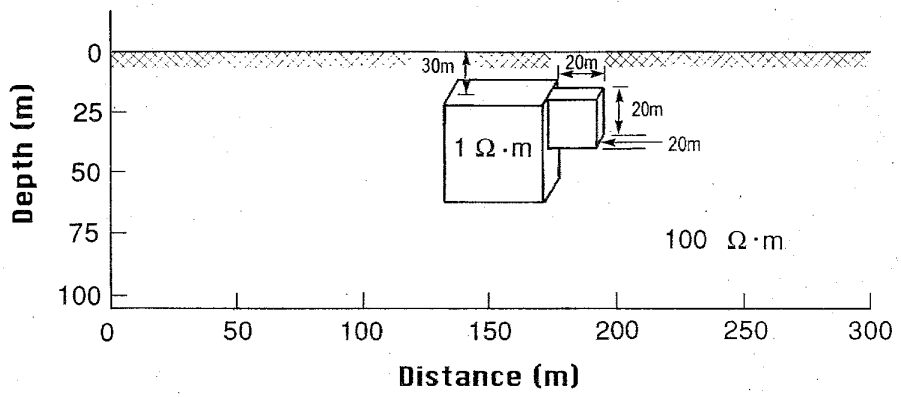

Fig. 3. Model B.

Again let γ be the conductivity of a background or an initial trial model and let $\gamma + \sigma$ be the conductivity of a perturbed medium. Assume that the n transmitter nodes are indexed by i and that $f = [f(1), f(2), \cdots, f(n)]^T$ is a vector of injection current intensities whose strength at node i is $f(i)$. The corresponding potentials are measured at m nodes. Thus u and w are the vectors of measured potentials for the media γ and $\gamma + \sigma$. An arbitrary current f and measured potentials u and w are related one to another through

$$u = Z_\gamma f \tag{5}$$

and

$$w = Z_{\gamma+\sigma} f \tag{6}$$

where Z_γ and $Z_{\gamma+\sigma}$ are the impedance matrices. Equations (5) and (6) are perfectly general and hold for any array of transmitter and receiver electrodes. To discuss the design of optimal arrays of transmitter electrodes, it is expeditious to introduce source basis vectors. We consider the case when the number of transmitter electrodes is equal to the number of receiver electrodes. We will define a set of basis vectors $\{j_k\}, k = 1, \cdots, n$, by $j_k = [j_k(1), j_k(2), \cdots, j_k(n)]^T$, where

$$j_k(i) = \begin{cases} 1, & \text{if } i = k \\ 0, & \text{otherwise.} \end{cases} \tag{7}$$

Thus the basis vector j_k defines a unit nodal current at transmitter node k.

The numerical entries of Z_γ and $Z_{\gamma+\sigma}$ can be immediatly identified in terms of the potential responses to the currents j_k from (5) and (6). Equation (5) shows that the measured potential vector u_k corresponding to the injection current j_k numerically equals the kth column of the impedance matrix Z_γ:

$$\begin{bmatrix} u_k(1) \\ u_k(2) \\ \cdots \\ u_k(k) \\ \cdots \\ u_k(n) \end{bmatrix} = \begin{bmatrix} z_{11} & \cdots & z_{1k} & \cdots & z_{1n} \\ & & z_{2k} & & \\ \cdots & & \cdots & & \cdots \\ z_{1k} & \cdots & z_{kk} & \cdots & z_{kn} \\ \cdots & & \cdots & & \cdots \\ & & z_{nk} & & \end{bmatrix} \begin{bmatrix} 0 \\ 0 \\ \cdots \\ 1 \\ \cdots \\ 0 \end{bmatrix}. \tag{8}$$

Here z_{ik} are the entries of the impedance matrix Z_γ.

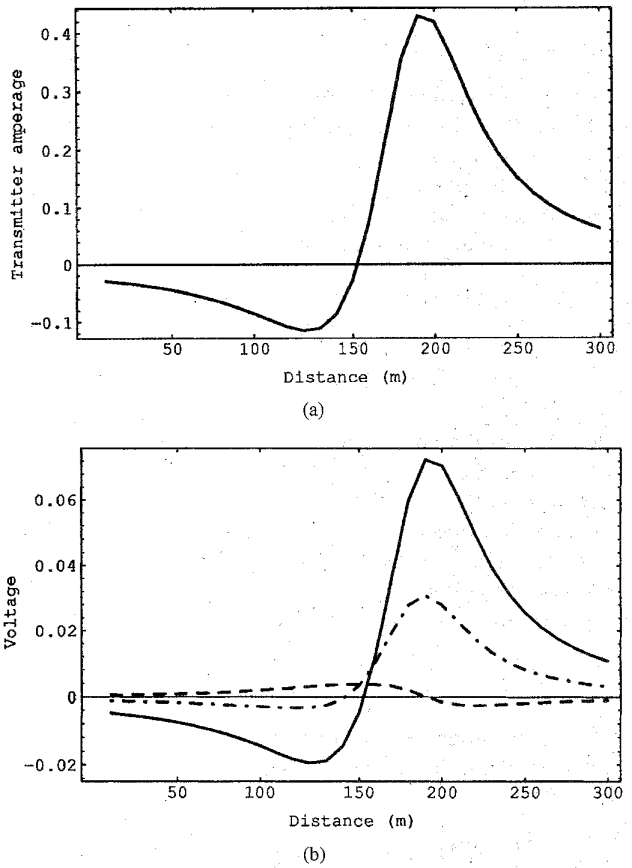

Fig. 4. Model B. A plot of the optimal transmitter (a) current intensity and (b) secondary responses for three different transmitter current patterns: 1) response of the optimal current (solid line); 2) response of the current of equal intensity at all electrodes (dot-dashed line); and 3) response of the unit current at the central electrode (dashed line).

It can be seen immediately from this equation that the kth column of Z_γ is numerically equal to the left hand side:

$$u_k(i) = \sum_{l=1}^{n} z_{il} j_k(l) = z_{ik}. \tag{9}$$

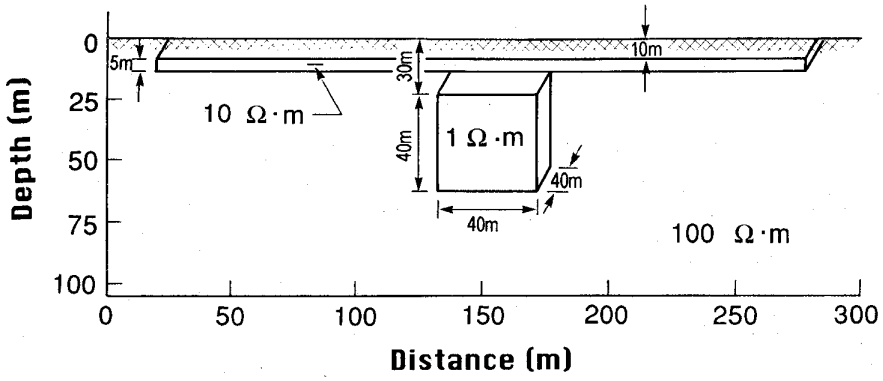

Fig. 5. Model C.

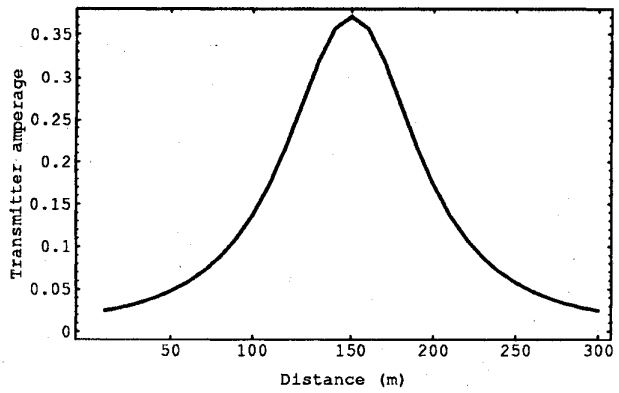

(a)

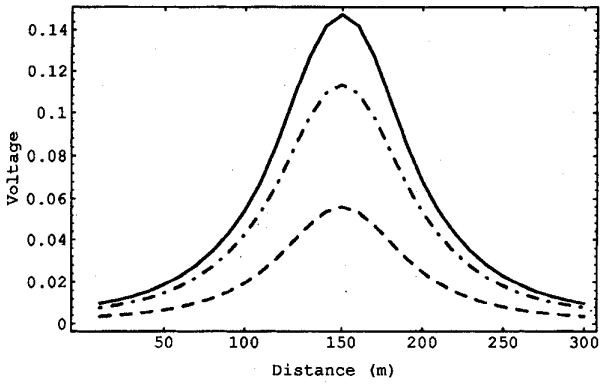

(b)

Fig. 6. Model C. A plot of the optimal transmitter (a) current intensity and (b) secondary responses for three different transmitter current patterns: 1) response of the optimal current (solid line); 2) response of the current of equal intensity at all electrodes (dot-dashed line); and 3) response of the unit current at the central electrode (dashed line).

Dimensionally

$$z_{ik} = u_k(i)[\text{volts}]/1[\text{amps}] = \hat{u}_k(i)[\text{ohms}]. \tag{10}$$

Therefore, the matrices Z_γ and $Z_{\gamma+\sigma}$ can be written as matrices with columns equal to $\hat{u}_k$ and $\hat{w}_k$, respectively. Thus,

$$Z_\gamma = \{\hat{u}_1, \hat{u}_2, \cdots, \hat{u}_n\} \quad \text{and} \quad Z_{\gamma+\sigma} = \{\hat{w}_1, \hat{w}_2, \cdots, \hat{w}_n\}. \tag{11}$$

Since the basis vectors $\{j_k\}, k = 1, \cdots, n$ span the space of all point current distributions, we can consider any current f distributed among the nodes as a weighted sum

$$f = \sum_{k=1}^{n} \alpha_k j_k \quad \text{where} \quad \sum_{k=1}^{n} \alpha_k^2 = 1. \tag{12}$$

The weights α_k are normalized to 1 to provide a basis for comparing different electrode arrays, since for any arbitrary array more transmitter power will of course lead to a greater voltage response.

For a current f the potential vector given by the background γ is

$$Z_\gamma f = Z_\gamma \left(\sum_{k=1}^{n} \alpha_k j_k \right) \tag{13}$$

while the potential vector measured over $\gamma + \sigma$ is

$$Z_{\gamma+\sigma} f = Z_{\gamma+\sigma} \left(\sum_{k=1}^{n} \alpha_k j_k \right). \tag{14}$$

Then

$$(Z_{\gamma+\sigma} - Z_\gamma) f = (Z_{\gamma+\sigma} - Z_\gamma) \sum_{k=1}^{n} \alpha_k j_k \tag{15}$$

represents the vector of anomalous potentials.

We now have the problem in a form which is amenable to mathematical analysis. Suppose we wish to find a source f which maximizes the response of a perturbation σ about an *a priori* conductivity model γ. Then we wish to find the set of coefficients $\{\alpha_k\}$ which solves the problem

$$M = \max_{\{\alpha_k\}:\, \sum_{k=1}^{n} \alpha_k^2 = 1} \left\| (Z_{\gamma+\sigma} - Z_\gamma) \sum_{k=1}^{n} \alpha_k j_k \right\| \tag{16}$$

where the norm is the Euclidean sum of squares.

Given an appropriate modeling algorithm, we can calculate the impedance matrices $Z_{\gamma+\sigma}$ and Z_γ or given measurements we can construct the impedance matrix $Z_{\gamma+\sigma}$ from the measured data. In this case (16) constitutes an eigenvalue problem.

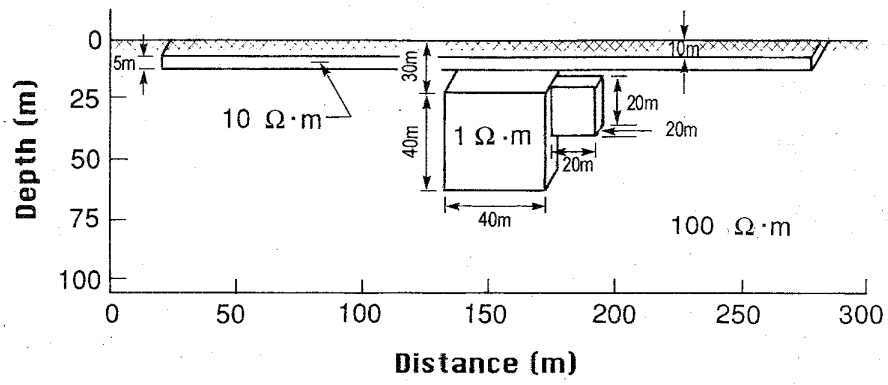

Fig. 7. Model D.

Let a vector α with components α_k be a vector of current intensities injected at different electrodes. The problem (16) states that

$$M = \max_{\alpha:\,\|\alpha\|=1} \|(Z_{\gamma+\sigma} - Z_\gamma)\alpha\|. \tag{17}$$

This problem is an eigenvalue problem for the matrix $Z_{\gamma+\sigma} - Z_\gamma$, its solution is the eigenvectors α and the eigenvalues M such that

$$\tilde{M}\alpha = (Z_{\gamma+\sigma} - Z_\gamma)\alpha \tag{18}$$

where $|\tilde{M}| = M$. This problem can be solved numerically. We solve it using a standard subroutine of Singular Value Decomposition (SVD) from LINPACK package [14]. Another way of solving the problem of maximization of the response based on the power method is utilized in the paper [10].

Equation (18) shows that the intensities of the optimal injected current $\{\alpha_k\}$, being a solution of the eigenvalue problem (17), are proportional to the values of the measured voltage difference

$$\tilde{M}\alpha_i = \sum_{k=1}^{n} (Z_{\gamma+\sigma}(i,k) - Z_\gamma(i,k))\alpha_k \tag{19}$$

where $Z_{\gamma+\sigma}(i,k)$ and $Z_\gamma(i,k)$ are the (i,k)th entries of the impedance matrices.

Thus the eigenvalue problem (17) has the solution

$$\{M_1, \alpha^1\}, \{M_2, \alpha^2\}, \cdots, \{M_n, \alpha^n\}, \quad \text{where} \quad \alpha^i = \{\alpha_k^i\} \tag{20}$$

which is found numerically.

The values M_i and the corresponding currents $J_i = \sum_k \alpha_k^i j_k$ form an eigensystem. These currents are orthogonal and can be used as a basis for any injection current pattern. The current J_1, which corresponds to the maximal eigenvalue M_1, gives the most amount of information about the inclusion. The remaining eigenvalues form a monotonically decreasing sequence. Using the injection currents corresponding to these eigenvalues will reveal more information about the model if the data are noise free, although the amount of information gained will diminish with each successive eigenvalue. If the data have noise, then there may be a value N such that for all $i > N$, eigenvalues M_i will be within the noise of the data in some statistical sense. In this case, using eigencurrents for $i > N$ will not lead to useful information concerning σ.

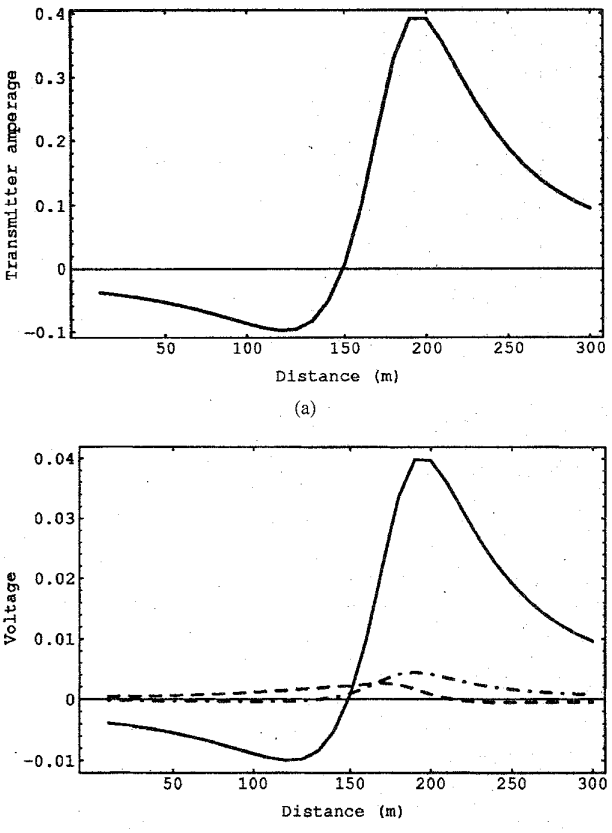

Fig. 8. Model D. A plot of the optimal transmitter (a) current intensity and (b) secondary responses for three different transmitter current patterns: 1) response of the optimal current (solid line); 2) response of the current of equal intensity at all electrodes (dot-dashed line); and 3) response of the unit current at the central electrode (dashed line).

It is useful to have a measure of the optimality of an arbitrary injection current. Since the eigencurrents are orthogonal, a measure of information content $\mathcal{I}$ (3) of an arbitrary current injection pattern f can be calculated as

$$\mathcal{I}^2 = \sum \kappa_i^2 M_i^2 \tag{21}$$

where κ_i are the coefficients of the expansion of the current f in terms of the eigencurrents J_i.

C. Physical Interpretation of the Optimal Current Electrode Array

We have shown how to design arrays which give a maximal response from a target inhomogeneity given an *a priori* background model. It is shown [13] that the current maximizing the response from the inclusion also maximizes the scattering current energy over the inclusion. This corresponds to the concentration of current in the vicinity of the inclusion.

Let us consider a linearized problem by assuming that the conductivity perturbation is small. The linearized equation is an equation for the scattering potential $v = w - u$, and is obtained from (1) and (2)

$$\begin{aligned} &\nabla \cdot \gamma \nabla u = 0 \text{ in } \mathcal{D},\ \gamma \frac{\partial u}{\partial n} = f \text{ on } \partial \mathcal{D} \\ &\nabla \cdot \gamma \nabla v = -\nabla \cdot \sigma \nabla u \text{ in } \mathcal{D},\ \gamma \frac{\partial v}{\partial n} = 0 \text{ on } \partial \mathcal{D}. \end{aligned} \tag{22}$$

Here f is the applied current injected at point electrodes (12) with intensity α_k at the kth electrode, u is a potential of the electrical field in the model background problem, and v is a fluctuation of the potential caused by the presence of the inclusion.

Analogously with (19), the coefficients $\{\alpha_k\}$ are proportional to the values of the measured voltage difference. Thus in the linearized problem

$$\alpha_i = \frac{v_i}{\tilde{M}}$$

and

$$v_i = \sum_{k=1}^{n} (Z_{\gamma+\sigma}(i,k) - Z_{\gamma}(i,k))\alpha_k. \tag{23}$$

Using this property of the optimal current and (22) we find the expression for the energy of the scattering current $\mathcal{E}_\sigma$. Thus

$$\begin{aligned} \left| \int_{\mathcal{D}} J_\sigma \cdot E dx \right| &= \left| \int_{\mathcal{D}} \sigma \nabla u \cdot \nabla u dx \right| \\ &= \left| \sum_{k=1}^{n} \alpha_k v_k \right| = M. \end{aligned} \tag{24}$$

Here we exploit (22) and (23) and the fact that $\sigma = 0$ on the boundary $\partial \mathcal{D}$. J_σ is the scattering current, $J_\sigma = \sigma \nabla u$, and E is the background electric field, so that the expression $\int_{\mathcal{D}} J_\sigma \cdot E dx$ is the energy $\mathcal{E}_\sigma$ of the scattering current.

Since the optimal current maximizes the value of M, (24) implies that it maximizes the energy of the scattering current

$$M^2 = \left\{ \int_{\mathcal{D}} J_\sigma \cdot E dx \right\}^2 = \left\{ \int_{\mathcal{D}_\sigma} J_\sigma \cdot E dx \right\}^2 = \mathcal{E}_\sigma^2 \tag{25}$$

where $\mathcal{D}_\sigma$ is a domain occupied by inclusion σ.

Thus the optimal current intensity distribution on the surface focuses current inside the earth to the vicinity of inclusion. This is the reason it maximizes the response from the target inclusion.

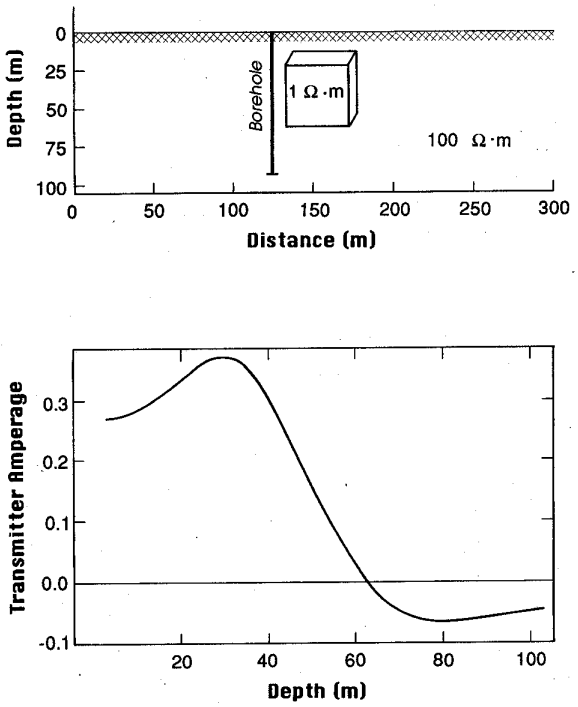

Fig. 9. Model E and a plot of optimal borehole transmitter current density for this model.

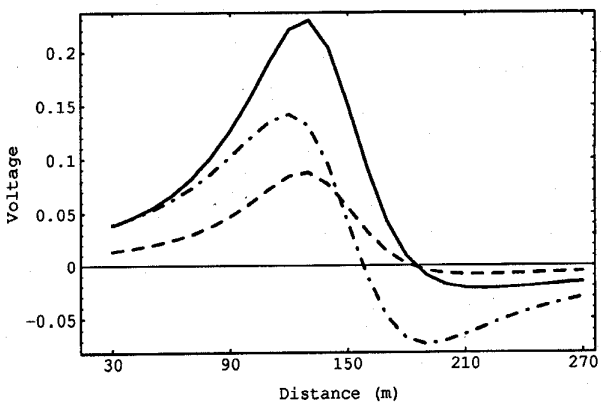

Fig. 10. Model E. Secondary voltage responses for three different borehole transmitter currents: 1) response of the optimal current (solid line); 2) response of the current of equal intensity at all electrodes (dot-dashed line); and 3) response of "the best" unit current for a single electrode (dashed line).

Fig. 14 in the next section shows current distributions inside the earth generated by the optimal current array designed for the particular problem of the detection of an inclusion, and by a conventional array.

III. Results of Computer Simulations

A. Models

We have conducted a number of computer simulations in order to check the theory and to show its application to some simple models. The models used in the calculations are the following.

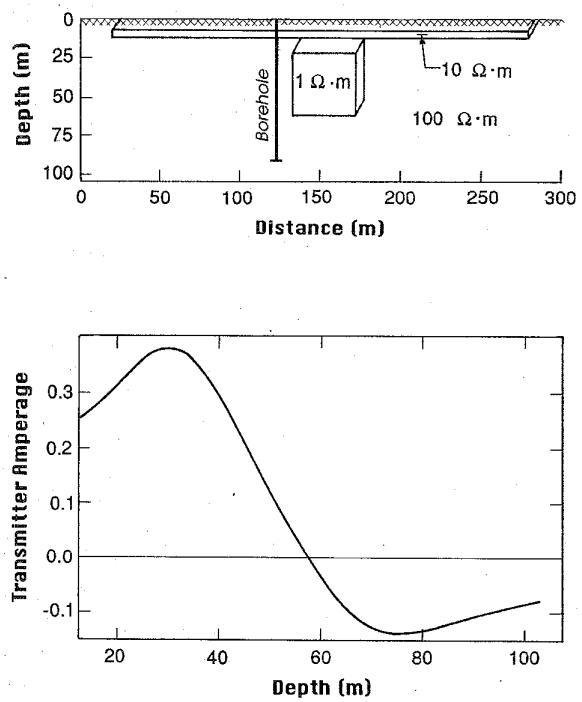

Fig. 11. Model F and a plot of optimal borehole transmitter current density for this model.

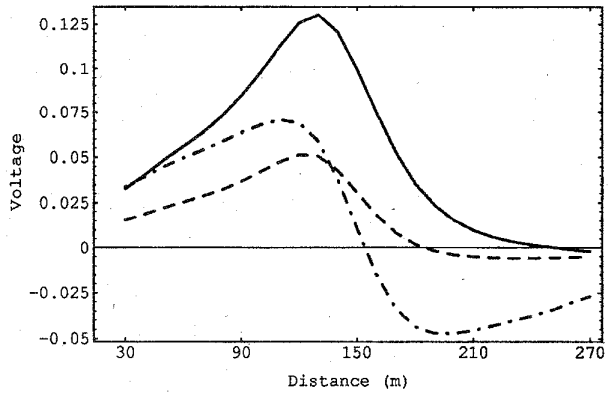

Fig. 12. Model F. Secondary voltage responses for three different borehole transmitter currents: 1) response of the optimal current (solid line); 2) response of the current of equal intensity at all electrodes (dot-dashed line); and 3) response of "the best" unit current for a single electrode (dashed line).

1) Model A: The background is a homogeneous halfspace of resistivity 100 $\Omega \cdot$ m, while the inhomogeneity is a cube 40 m $\times$ 40 m $\times$ 40 m, located at a depth of 30 m. The resistivity of the inclusion is 1 $\Omega \cdot$ m. The model is shown in Fig. 1.

2) Model B: The background for the model B is model A. The inclusion is an additional smaller sized cube of resistivity 1 $\Omega \cdot$ m. The size of the inclusion is 20 m $\times$ 20 m $\times$ 20 m, while the depth to its top is 30 m. Model B is depicted in Fig. 3.

3) Models C and D: Models C and D are similar to the models A and B with the difference that the background medium is a layered earth with a 10 $\Omega \cdot$ m layer of thickness 5 m, embedded in a 100 $\Omega \cdot$ m halfspace at a depth of 10 m. Models C and D are illustrated in Figs. 5 and 7, respectively.

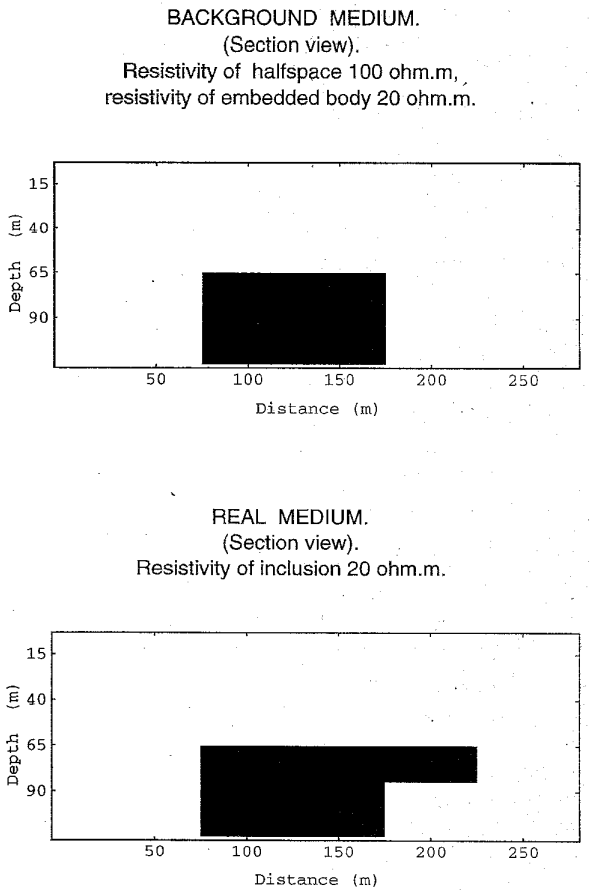

Fig. 13. Cross section of models used for illustrating current focusing. The embedded body in the background model is 100 m $\times$ 50 m $\times$ 50 m, while the inclusion is a 20 m thick body located near the background body.

4) Models E and F: Models E and F are similar to the models A and C with the difference that transmitter electrodes are located in a borehole. Models E and F are illustrated in Figs. 9 and 11, respectively.

B. Calculations

For every model for a given possible set of transmitter electrode positions, we calculate responses of the background medium and of the disturbed medium for three different types of excitation using an integral equation 3-D program [15].

The first excitation is the optimal current distribution with different intensities of the injected currents at different electrodes, with unit total intensity. The optimal current is designed specially for every model. It is the current pattern that maximizes the response from the target inclusion.

The second type of applied current is a current of equal intensity at all electrodes, also with unit total intensity.

The third type is a unit current concentrated at the electrode which gives a maximal response for a single transmitter electrode site.

Models A–D were used for investigating optimal surface transmitter current patterns. In each of these cases, a profile

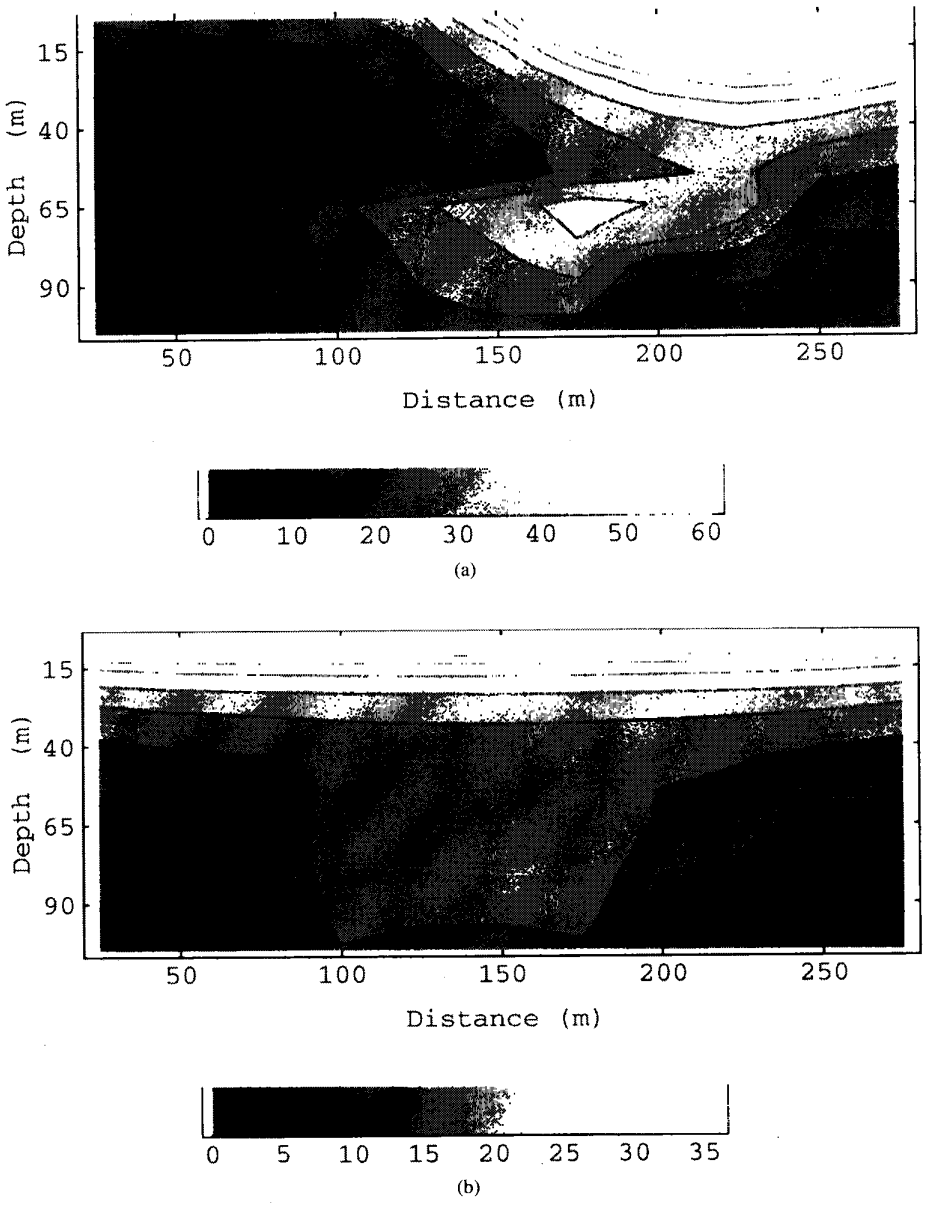

Fig. 14. Current distribution in the vicinity of the inclusion shown on the previous figure, for a focused transmitter current and for a uniform transmitter current intensity.

of 31 possible electrode positions straddled the center of the inhomogeneity in a vertical plane of symmetry. Figs. 1 through 8 present cross sections of the particular models, optimal injection current patterns along the traverse, and comparisons of the secondary response of the optimal currents and the suboptimal currents. From each of these figures, it is apparent that the optimal current utilizes the *a priori* structure in directing current to the perturbation. This is exactly the behavior which we would expect from our theory.

Models E and F were used to investigate the applications of the theory to borehole-to-surface measurements. In these cases, the sources are located in a vertical borehole 10 m from the left hand side of the inclusion while voltages are measured along a surface traverse in a vertical plane of symmetry of the inclusion. Here again, the optimal array focuses current into the region of the inhomogeneity. In Fig. 11, for example, the injected current is dipolar, with current being focused through the inclusion.

As in the case of the surface measurements, the secondary responses for the optimal injection current pattern is clearly superior those of the suboptimal injection currents.

C. Concentration of the Current to the Region of Inclusion

We will now give a numerical illustration of concentration of the current to the region of inclusion. Consider the models given in Fig. 13. Background consists of a 100 m × 50 m × 50 m 20 $\Omega \cdot$m body buried 65 m deep in a 100 $\Omega \cdot$m half-space. An inclusion has been placed near the main body. The

dimensions of the inclusion are 50 m × 50 m × 20 m, while its resistivity is 20 Ω · m.

Fig. 14 illustrates a contour of total current in a cross section of the background and inclusion, both for the focused array and for an array of equal current intensity. As shown, the focusing current concentrates energy in the vicinity of the inclusion, thus increasing the resolution of the inclusion. In this and all other numerical experiments, it should be emphasized that the background structure is known, but the only information concerning the inclusion is its measured impedance matrix.

IV. Conclusion

The problem and its solution can be viewed from different points. Suppose that we know approximately what sort of inclusion is under consideration. Then given an appropriate forward modeling algorithm we can calculate the impedance matrices and find the corresponding eigencurrents numerically. In this case we numerically simulate a problem which is similar to a real one, and having solved it we obtain the optimal current patterns to use in a real situation. Another application assumes that we know nothing about the inclusion but its measured impedance matrix. In this case we can use the measured impedance matrix and find the optimal current intensity distribution over the electrodes, thus designing the optimal array vis-à-vis the hypothesized *a priori* model. Lastly, since optimal currents focus energy in the region of the inclusion we can use this method as an imaging technique.

Acknowledgment

The authors are thankful to R. V. Kohn for numerous and fruitful discussions of the mathematical background of the problem which have made this work possible. They also thank the Consortium for Electromagnetic Modeling and Inversion for furnishing the 3-D forward modeling software used in this study.

References

[1] H. G. Doll, "Introduction to induction logging and application to logging of wells drilled with oil base mud," *Petrol. Trans. AIME*, vol. 186, pp. 148–162, 1949.

[2] ——, "The Laterolog: A new resistivity logging method with electrodes using an automatic focusing system," *Petrol. Trans. AIME*, vol. 192, pp. 305–316, 1951.

[3] ——, "Microlaterolog," *Petrol. Trans. AIME*, vol. 198, pp. 17–32, 1953.

[4] P. D. Jackson, "Focused electrical resistivity arrays: Some theoretical and practical experiments," *Geophys. Prospecting*, vol. 99, pp. 601–626, 1981.

[5] E. Brizzolary and M. Bernabini, "Comparison between Schlumberger electrode arrangement and some focused electrode arrangements in resistivity profiles," *Geophys. Prospecting*, vol. 27, pp. 233–244, 1979.

[6] D. H. Davies, O. Faivre, M.-T. Gounot, B. Seeman, J.-C. Trouiller, D. Benimeli, A. E. Ferreira, D. J. Pittman, J.-W. Smits, M. Randrianavony, B. I. Anderson, and J. Lovell, "Azimuthal resistivity imaging: A new generation laterolog," SPE 24676, presented at the 67th SPE Annu. Conf., Washington, DC, 1992.

[7] J. O. Parra and T. E. Owen, "Synthetically focused resistivity for detecting deep targets," in *Geotechnical and Environmental Geophysics*, S. H. Ward, Ed, vol. III. Tulsa, OK: SEG, 1990, pp. 37–50.

[8] L. P. Beard and A. C. Tripp, "Investigating the resolution of IP arrays using inverse theory," *Geophysics*, vol. 60, no. 5, pp. 1326–1341, 1995.

[9] D. Isaacson, "Distinguishability of conductivities by electric current computed tomography," *IEEE Trans. Med. Imag.*, vol. MI-5, pp. 91–95, 1986.

[10] D. G. Gisser, D. Isaacson, and J. C. Newell, "Theory and performance of an adaptive current tomography system," *Clin. Phys. Physiol. Meas.*, vol. 9, Suppl. A, pp. 35–41, 1988.

[11] D. Isaacson and M. Cheney, "Current problems in impedance imaging," in *Inverse Problems in Partial Differential Equations*, D. Colton, R. Ewing, and W. Rundell, Eds. Philadelphia, PA: SIAM, 1990, pp. 141–149.

[12] D. G. Gisser, D. Isaacson, and J. C. Newell, "Electric current computed tomography and eigenvalues," *SIAM J. Appl. Math.*, vol. 50, pp. 1623–1624, 1990.

[13] E. Cherkaeva and A. C. Tripp, "On the resolution of geoelectric imaging," submitted to *SIAM J. Appl. Math.*

[14] J. J. Dongarra, J. R. Bunch, C. B. Moler, and G. W. Stewart, *LINPACK User's Guide*, SIAM, 1979.

[15] C. W. Beasley and S. H. Ward, "Three-dimensional mise-a-la-masse modeling applied to mapping fracture zones," *Geophysics*, vol. 51, no. 1, pp. 98–113, 1986.

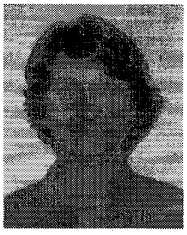

Elena Cherkaeva received the M.S. degree in mathematics in 1977 and the Ph.D. degree in mathematics and physics in 1988, both from Leningrad University, Russia.

From 1978 to 1991, she was with the Institute of Terrestrial Magnetism, Ionosphere and Radiowave Propagation, Academy of Sciences, Russia. She worked on problems of transformations of potential magnetic field for the purpose of magnetic cartography and magnetic prospecting, which include problems of numerical solution of PDE, statistical and asymptotical analysis, and regularization of ill-posed inverse problems. Since 1992, she has been with the University of Utah, Salt Lake City. Her main interests at present include high resolution geoelectric and induced polarization problems, optimal control of excitation sources for increasing geoelectrical resolution, inverse solution reliability, and nondestructive testing using noisy measurements.

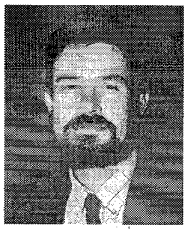

Alan C. Tripp earned the B.A. degree in mathematics from Michigan State University, East Lansing, and the M.S. and Ph.D. degrees in geophysics from the University of Utah, Salt Lake City.

He has been with ARCO and the University of Utah in various positions. At present, he is a Research Associate Professor of Geophysics at the University of Utah.